

PACS numbers: 81.15.Ef, 75.70.Ak, 75.61. – r

MAGNETIC AND LOW TEMPERATURE CONDUCTIVITY STUDIES IN OXIDIZED NANO Ni FILMS

*P.J. Sadashivaiah*¹, *T. Sankarappa*¹, *T. Sujatha*², *P. Saravanan*³,
*Santoshkumar*¹, *M. Prashantkumar*¹, *G.B. Devidas*¹, *B. Vijayakumar*¹,
*N. Nagaraja*¹, *N. Sharanabasava*¹

¹ Department of Physics, Gulbarga University,
Gulbarga, Gulbarga 585 106, India
E-mail: sankarappa@rediffmail.com

² H.P.S. Kalkhora, Basavakalyan (Tq), Bidar (Dt), India

³ Defence Metallurgical Research Laboratory,
Kanchanbagh, Hyderabad, A.P. 500 058, India

A set of single layered nanostructured Ni films of thickness, $t = 25$ nm, 50 nm, 75 nm and 100 nm have been deposited using electron beam gun evaporation technique at 473 K under high vacuum condition. From the grazing incidence X-ray diffraction (GIXRD) studies, NiO phase formation has been noted. Grain sizes of the films were determined. The microstructure was examined by scanning electron microscope (SEM) studies. Average surface roughness was determined by atomic force microscope (AFM). The room temperature magnetization has been measured using the vibrating sample magnetometer (VSM). The coercive field was observed to be increasing with increasing t and became maximum for $t = 75$ nm and decreases for further increase in t . The behavior of coercive field with t indicated softness of the films. Low temperature electrical conductivity in the range from 5 K to 300 K has been measured. Temperature dependence of electrical conductivity showed semiconducting behavior. At temperatures above $\theta_D/2$ (θ_D is the Debye temperature), the conductivity behavior has been understood in the light of Mott's small polaron hopping model and activation energies were determined. An attempt has been made to understand conductivity variation below $\theta_D/2$ using variable range hopping models due to Mott and Greaves.

Keywords: THIN FILMS, SURFACE ROUGHNESS, MAGNETIZATION,
COERCIVE FIELD, CONDUCTIVITY.

(Received 24 August 2011, in final form 18 October 2011
published online 30 December 2011)

1. INTRODUCTION

Research on thin metallic films led to the discovery of films of numerous scientific and technological applications. Nickel oxide (NiO) is an important material because of its interesting structural, magnetic and electrical properties. It has been considered as antiferromagnetic [1] and also treated as a p-type semiconductor because of its wide band gap [2]. It is used in a variety of electronic devices [3-6]. NiO films have been fabricated by different physical and chemical vapor deposition techniques [7], plasma

enhanced chemical vapor deposition [8], RF magnetron sputtering [9,10] and electron beam evaporation [11]. Substrate temperature effects on structural, electrical and mechanical properties were investigated [12-14]. Effect of crystallographic orientations on electrical properties were studied [15]. The structural and magnetic properties of NiO films showed that these properties are very sensitive to the degree of oxidation [16]. The detailed studies of structure, surface morphology, magnetic and low temperature electrical properties of NiO films have not been reported so far.

In the present article, we report the investigations on structural, magnetic and low temperature electrical properties of Ni films of thickness, 25 nm, 50 nm, 75 nm and 100 nm.

2. EXPERIMENTAL

The single nanostructured Ni films were prepared using the electron beam gun technique at a pressure of 5×10^{-6} mbar. The films were deposited on to the glass substrates held at a temperature of 473 K. Before deposition, the glass substrates were kept immersed for half an hour in boiling chromic acid solution and then left them for 10 hours in the solution. After that they were washed with detergent soap solution and finally rinsed with acetone. Before loading into the vacuum chamber, they were again cleaned and dried. The nickel layer was deposited by evaporating the nickel from a molybdenum crucible. The thickness of the layer was measured during deposition using quartz crystal thickness monitor. The films were annealed to room temperature in the vacuum chamber.

Structural investigations were carried out by grazing incidence X-ray diffraction (GIXRD) studies using Bruker-D8 advance diffractometer with Cu-K α radiation of 1.5406 Å wavelength. The microstructure of the films was probed using (FEI Quanta 400) Scanning Electron Microscope. Surface morphology of the films at nanometric scale has been investigated by AFM (Digital Instruments Nanoscope III). Average surface roughness of the films were determined on a scan area of $1 \mu\text{m} \times 1 \mu\text{m}$ using Nanoscope software. Room temperature magnetization was measured using vibrating sample magnetometer (Model ADE-EV9) with a maximum applied field of 0.3 T. The electrical conductivity measurements were carried out by four point method using an Oxford Instruments make conductivity setup in the temperature range from 5 K to 300 K.

3. RESULTS AND DISCUSSION

3.1 Grazing incidence X-ray diffraction (GIXRD) studies

The GIXRD spectra of the films obtained for 2θ between 38° and 49° for NiO films are shown in Fig. 1 and the Gaussian fit to the peaks are also depicted. The spectra consists of single broad peak and it has been indexed according to ICDD file cards. The peak position noted for N2, N3 and N4 films does not any match planes in Ni and Ni₂O₃ and match with plane (200) in NiO. It infers that these films got naturally oxidized and converted into NiO films. The peak position noted for N1 film has got more uncertainty. The peaks were observed to be getting sharpened with increasing film thickness and this can be seen in terms of peak widths mentioned in Table 1. It indicates that crystallinity is improving with the thickness of the films.

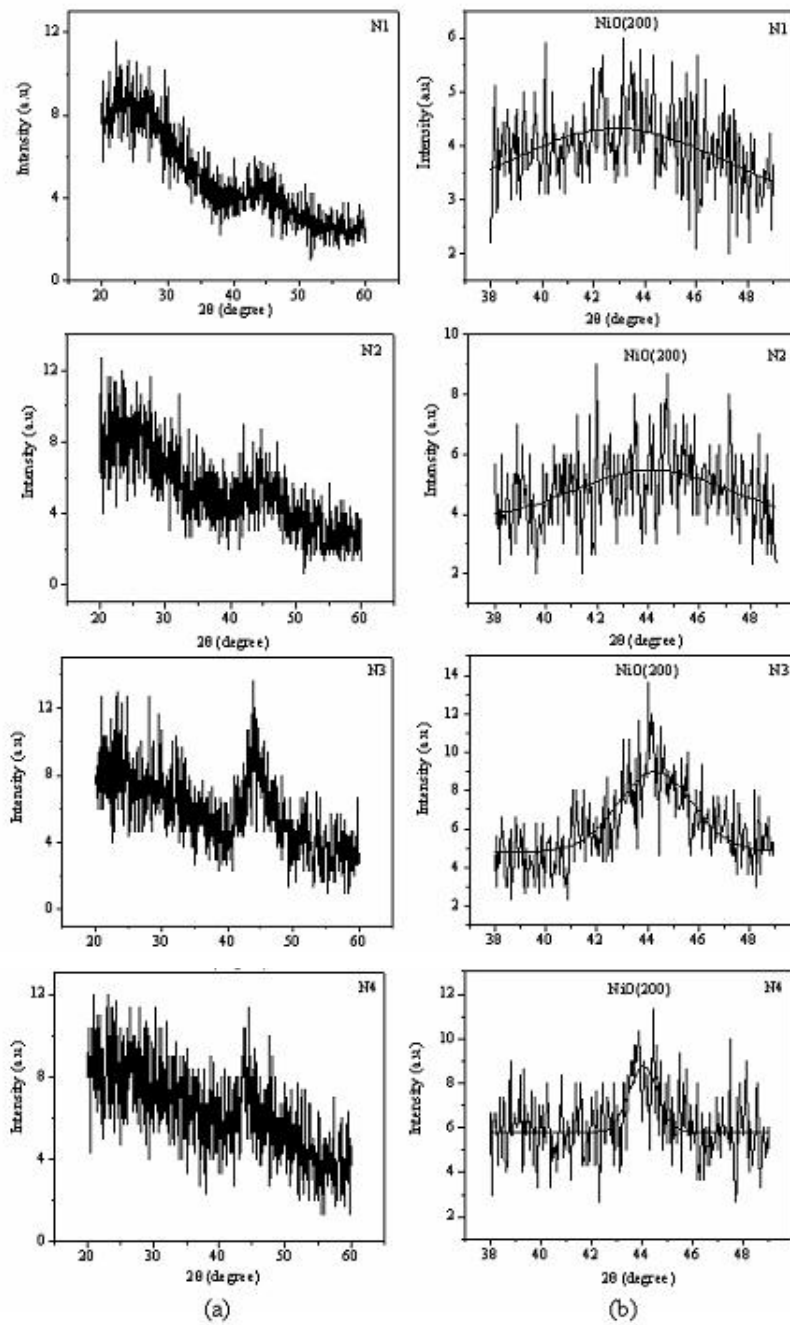


Fig. 1 – GIXRD spectra for films (a) and the spectra around the peaks (b). The solid line are the Gaussian fits to the peak

The oxidation state of NiO has also been observed in ref [17] for the films annealed at 823 K.

The average grain sizes were determined using Scherrer's formula [18],

$$D = 0.9\lambda/(B\cos\theta_B)$$

where D is the grain size, B the angular width in terms of 2θ , $2\theta_B$ the Bragg angle and λ the wavelength of X-rays. The interplanar spacing, d was calculated using the relation,

$$d = 0.5\lambda/\sin\theta_B$$

From the structure of the spectra around the peak, the grain sizes, D , and interplanar spacings, d , were determined. The D values thus obtained inform that the present films are nanocrystalline in nature. The grain size increases with increasing thickness of the films (Fig. 2). Other parameters extracted from the GIXRD spectra are recorded in Table 1.

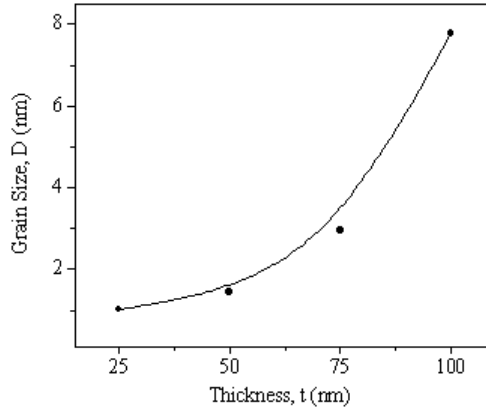


Fig. 2 – Grain size, D , versus thickness, t . Solid line shown is a guide to the eye

Table 1 – Parameters extracted from the GIXRD spectra

Films	Peak position (2θ)	Peak width	Interplanar spacing, d (Å)
N1	42.90	8.28	2.10
N2	44.11	5.94	2.05
N3	44.31	2.90	2.04
N4	44.02	1.10	2.05

3.2 Scanning electron microscopy (SEM) studies

The microstructure of the films examined using SEM with in the scan range of 1 μm . A typical SEM image of N1 film is shown in Fig. 3. The images of all the four films appear smooth, compact and fine in structure which indicates a high content of nanocrystalline particles. Individual particles could not be measured for sizes due to their high density packing.

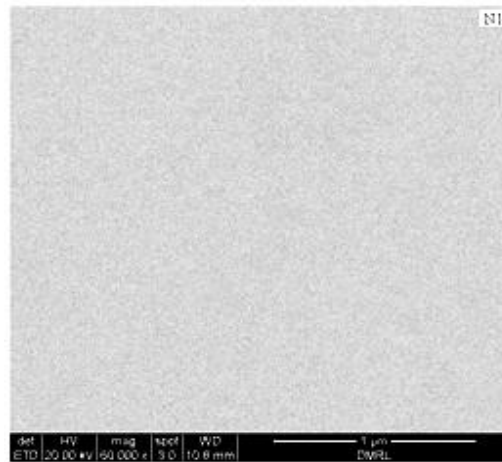


Fig. 3 – SEM image taken on N1 film

3.3 AFM studies

In order to investigate surface morphology of the films, AFM images with a scan area of $1\ \mu\text{m} \times 1\ \mu\text{m}$ have been recorded. The AFM images in 2D and 3D for the film N4 is shown in Fig. 4. The self-assembly of spherical nanocrystals can be observed in the AFM images.

The AFM images have been quantified by recording the height, h , versus distance, x , profiles across the length (white lines drawn in Fig. 4a) as shown in Fig. 5 [19]. This analysis provided information about average surface roughness, h (pair of blue dot lines in Fig. 4(a)) of the films. The t dependence of h is plotted in Fig. 6. It is observed in this figure that the surface roughness increases with t up to 75 nm and started smoothing for higher t .

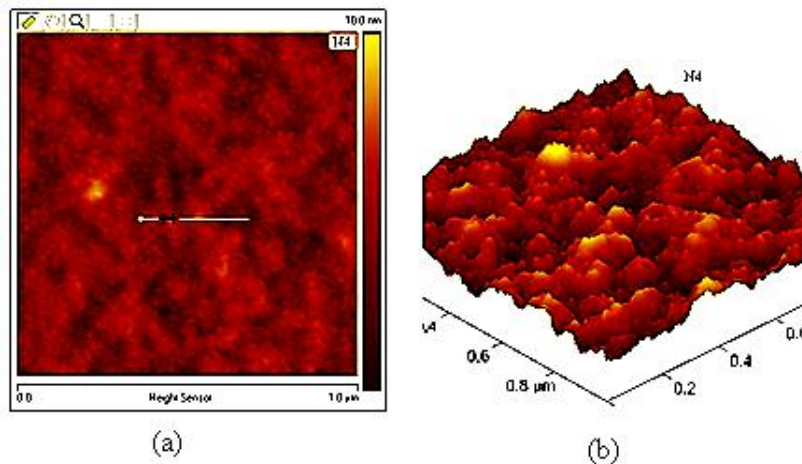


Fig. 4 – AFM images of N4 film in 2D (a) and 3D (b)

The sectional analysis carried out using the software Nanoscope on the AFM images of all the films indicated that the grain height changes considerably over the distance [20]. Therefore, h for each of the films has been worked out by measuring them at different cross sections of the image and then averaged.

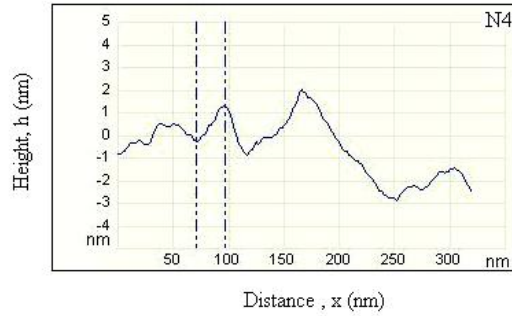


Fig. 5 – Height, h , versus distance, x , profile for N4 film along the white line drawn in Fig. 4(a)

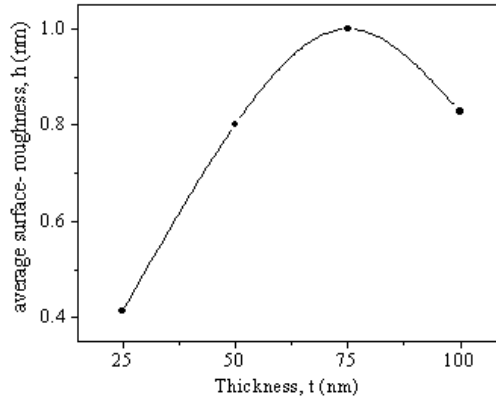


Fig. 6 – Average surface roughness, h , versus thickness, t , for the films. The solid lines shown is a guide to the eye

3.4 Magnetization

The magnetization, M , as function of applied field, H , was measured at room temperature by applying field parallel to the surface of the films. The recorded hysteresis loops are shown in Fig. 7. The coercive field, H_c and remanent magnetization, M_r , were extracted from these hysteresis loops. The film thickness dependence of these parameters is plotted in Fig. 8.

The bulk Ni is well known to be ferromagnetic and the Ni films exhibited well defined hysteresis loops with low H_c values, less than 0.005 T [21]. Whereas NiO was considered to be antiferromagnetic, which is in agreement with our result. No saturation magnetization has been observed for the present films. For fields above 0.1 T, magnetization of the present films decreased with field and it is expected to be due to oxidation of the films leading to the formation of NiO phase.

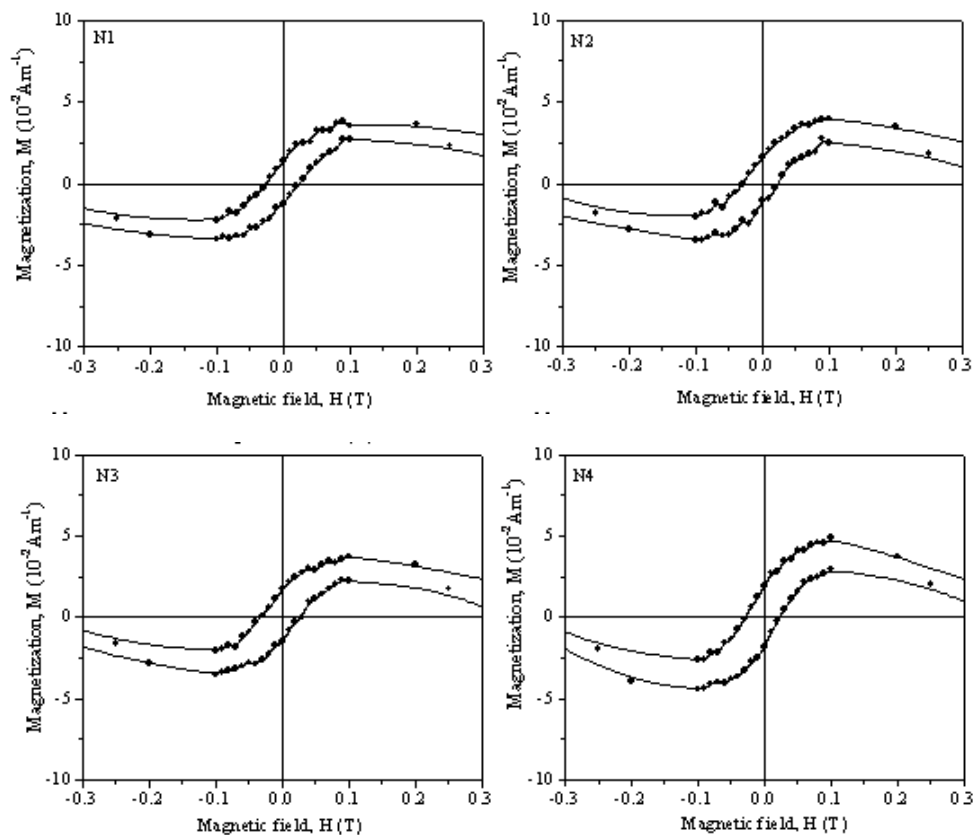


Fig. 7 – M - H loops of the films. The solid lines are B-spline fits to the data and are shown to guide the eye.

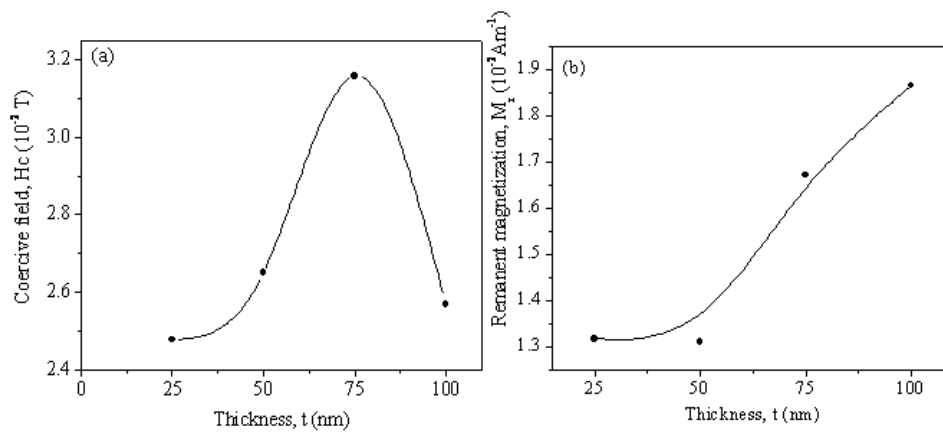


Fig. 8 – Thickness, t , dependence of (a) coercive field (H_c) and (b) remanent magnetization (M_r) for the films. The solid lines shown are guides to the eye

The H_c is found to be increasing with increase of t up to 75 nm and slowly decreased thereafter. The decrease in H_c after 75 nm indicates that the film got softened [22]. This can be due to decrease in average surface roughness for films of thickness above 75 nm (Fig. 6). The variation of M_r with t can be associated with grain growth [23].

3.5 Electrical Conductivity

The electrical conductivity, σ , in the range temperature, T , from 5 K to 300 K has been measured. The measured variation of σ with T for N1 film is depicted in Fig. 9. The similar nature of variation of σ with T has been observed for the remaining films. The conductivity increased with increasing t . The temperature dependence of conductivity reveals semiconducting type of behavior. The measured conductivities at room temperature are in good agreement with similar thin NiO films [24]. However, the room temperature conductivity of the present films is higher than that of thick NiO films and NiO nanocrystals [25, 26].

In bulk NiO, for temperatures below 1000 K, two competing mechanisms contribute to the conductivity; one due to small polarons in the 3d band of Ni^{2+} and the other due to large polarons in the 2p band of O^{2-} [27]. For temperature above 100 K, small polarons conduct by means of thermally activated hopping with small activation energy [28-30]. In the temperature range of 200 – 1000 K, the band like conduction due to large polarons in the 2p band of O^{2-} with higher activation energy dominates [27].

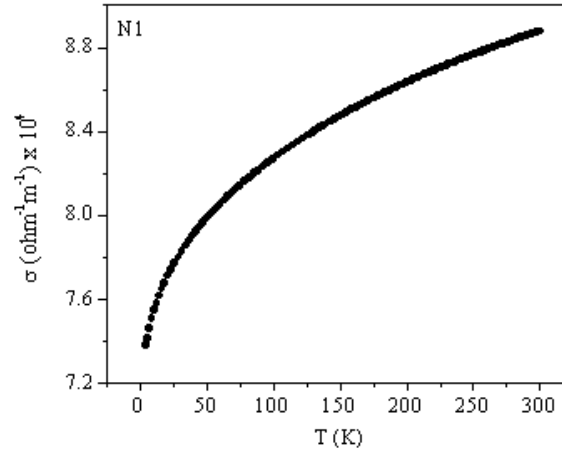


Fig. 9 – Conductivity, σ versus temperature, T for N1 film in the entire experimental range of temperature

According to the Mott's small polaron hopping model, the electrical conductivity is expressed as [31],

$$\sigma = (\sigma_0/T) \exp(-\Delta E/k_B T)$$

where ΔE is the activation energy.

The Mott's plots of $\ln(\sigma T)$ versus $(1/T)$ plots are shown Fig. 10. The curves are linear at high temperature and deviates from linearity below $\theta_D/2$, where θ_D is Debye temperature. The least square linear lines were fit to the data for temperatures above $\theta_D/2$. From the slopes, the activation energy, ΔE , were estimated and recorded in Table 2. The ΔE values are in the range 21.8 meV to 22.9 meV and they are smaller than that reported for NiO films and nanocrystals [24-26].

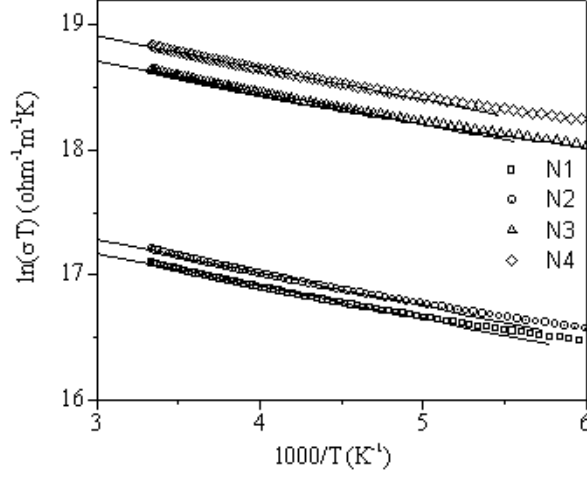


Fig. 10 – Mott's SPH plots of $\ln(\sigma T)$ versus $(1000/T)$ for films. Solid lines shown are the linear fits for $T > (\theta_D/2)$

For the data below $\theta_D/2$, we attempted to apply the variable-range-hopping (VRH) models proposed by Mott [32] and Greave [33]. In Mott's VRH model, the conduction is based on a single optical phonon approach and the conductivity is expressed as,

$$\sigma = A \exp(-T_0 / T)^{1/4},$$

where

$$T_0 = 256 \left[2\alpha^3 / 9\pi k_B N(E_F) \right],$$

and

$$A = \left[e^2 / 2(8\pi)^{1/2} \right] v_0 \left[N(E_F) / \alpha K_B T \right]^{1/2},$$

where $N(E_F)$ is density of states at the Fermi level.

A and T_0 are obtained from the $\ln(\sigma)$ versus $T^{-1/4}$ plots shown in Fig. 11. It is commonly held that much use of the exponent T_0 has been made to extract values of $N(E_F)$, given assuming value for $\alpha = 10 \text{ nm}^{-1}$ [34, 35]. The $N(E_F)$ values obtained are shown in Table 2. These $N(E_F)$ values are much higher than that quoted for NiO nanocrystals [26]. We further applied Greaves VRH model [33], at low temperature.

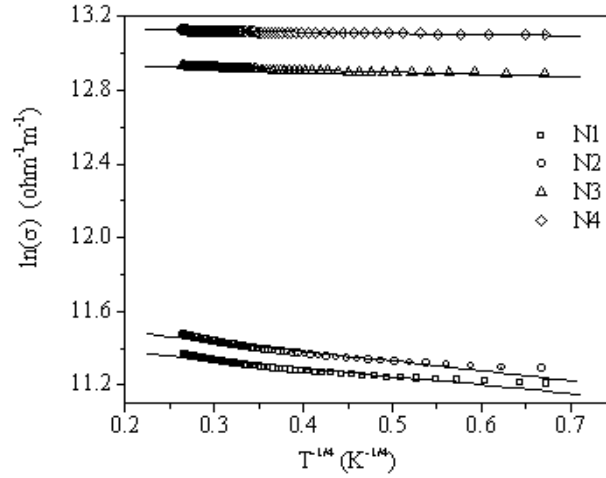


Fig. 11 – Mott's VRH plots of $\ln(\sigma)$ versus $T^{-1/4}$ for the films. Solid lines shown are the linear fits for $T < (\theta_D/2)$

Accordinging this model, conductivity is given by

$$\sigma T^{1/2} = B \exp(-T_0/T)^{1/4}$$

Where

$$T_0 = (2.1)^4 \left[\alpha^3 / k_B N(E_F) \right]$$

The Greaves plots of $\ln(\sigma T^{1/2})$ versus $T^{-1/4}$ are shown in Fig. 12. The fit parameters obtained are also shown in Table 2. The $N(E_F)$ values thus obtained are also much higher than that reported in reference [26]. Both the VRH models appear to fit well with the data. However, $N(E_F)$ values derived from them are abnormally high. It can therefore be concluded that low temperature conductivity of the present films can not be satisfactorily explained using both Mott's and Greaves VRH models.

Table 2 – Parameters extracted from the conductivity data

Film	ΔE (meV)	θ_D (K)	Mott's (VRH) Greaves (VRH)	
			$N(E_F)$ (eV ⁻¹ cm ⁻³)	$N(E_F)$ (eV ⁻¹ cm ⁻³)
N1	22.7	403.1	5.23×10^{30}	2.63×10^{26}
N2	22.9	404.8	2.54×10^{30}	2.37×10^{26}
N3	21.9	415.0	1.0×10^{33}	3.21×10^{26}
N4	21.8	420.4	1.01×10^{34}	3.45×10^{26}

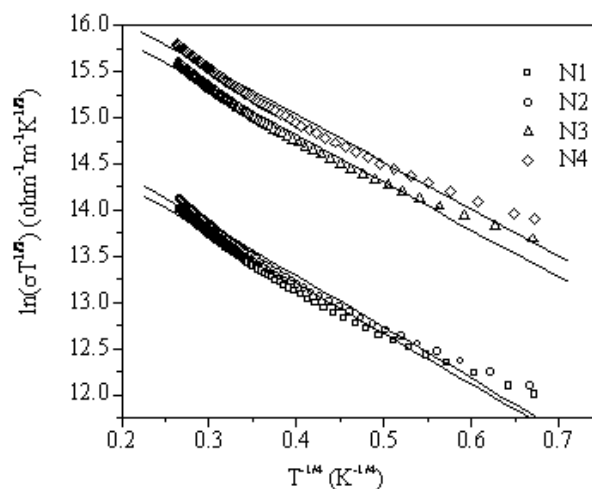


Fig. 12 – Greaves VRH plots of $\ln(\sigma T^{1/2})$ versus $T^{-1/4}$ for the films. Solid lines shown are the linear fits for $T < (\theta_D/2)$

4. CONCLUSION

A set of single nanostructured Ni films of thickness were deposited using electron beam gun evaporation technique at under high vacuum conditions. The NiO phase formation in the films has been detected through GIXRD studies. Surface roughness values have been determined from AFM data.

At room temperature, magnetic hysteresis loops were recorded in a vibrating sample magnetometer. The M-H curves do not reflect perfect ferromagnetism. It is concluded that the present films are antiferromagnetic and that may be due to the formation of NiO phase.

Low temperature electrical conductivity has been measured. Temperature dependence of electrical conductivity show semiconducting behavior. At temperatures above $\theta_D/2$, the conductivity has been analyzed in the light of Mott's small polaron hopping model. The conductivity data below $\theta_D/2$ could not be explained by VRH models due to Mott and Greave.

ACKNOWLEDGEMENT

One of the authors, T. Sankarappa acknowledges the rigorous research training that he received from Professor Mike Springford and Dr. P.J. Meeson at H.H. Wills Physics Laboratory, University of Bristol, UK.

REFERENCE

1. E. Fujii, A. Tomozawa, H. Torii, R. Takayama, *Jpn. J. Appl. Phys.* **35**, L328 (1996).
2. H. Sato, T. Minami, S. Takata, T. Yamada, *Thin Solid Films* **236**, 27 (1993).
3. C.G. Granqvist, *Handbook of inorganic electrochromic materials* (Amsterdam, The Netherlands: Elsevier Science: 1995).
4. E. Avendano, L. Berggren, G.A. Niklasson, C.G. Granqvist, A. Azens, *Thin Solid Films* **496**, 30 (2006).
5. C.K. Romana, B. Peter, *Acta Chim. Slov.* **53**, 136 (2006).

6. K.D. Lee, W.C. Jung, *J. Korean Phys. Soc.* **45**, 447 (2004).
7. P. Puspharajah, S. Radhakrishna, A.K. Arof, *J. Mater. Sci.* **32**, 3001 (1997).
8. W.C. Yeh, M. Matsumura, *Jpn. J. Appl. Phys.* **36**, 6884 (1997).
9. H.-L. Chen, Y.-M. Lu, W.-S. Hwang, *Surf. Coat. Tech.* **198**, 138 (2005).
10. S. Nandy, U.N. Maiti, C.K. Ghosh, K.K. Chattopadhyay, *J. Phys.: Condens. Mater* **21**, 115804 (2009).
11. T. Seike, J. Nagai, *Sol. Energ. Mater.* **22**, 107 (1991).
12. I. Fasaki, A. Koutoulakia, M. Kompitsasb, C. Charitidis, *Appl. Surf. Sci.* **257**, 429 (2010).
13. B. Sasi, K.G. Gopchandran, *Sol. Energ. Mat. Sol. C.* **91**, 1505 (2007)
14. B. Sasi, S. Sankar, K.M. Nissamudeen, G. Rajan, A.H. Bahna, K.G. Gopchandran, *J. Optoelectron. Adv. M.* **10**, 2637 (2008)
15. H.-L. Chen, Y.-Sh. Yang, *Thin Solid Films* **516**, 5590 (2008).
16. Y.K. Seo, D.J. Lee, Y.-D. Koh, J.-S. Chung, Y.S. Lee, Y. Jo, *J. Phys. D.: Appl. Phys.* **42**, 115407 (2009).
17. B. Sasi, K.G. Gopchandran, P.K. Manoj, P. Koshy, P. Prabhakara Rao, V.K. Vaidyan, *Vacuum* **68**, 149 (2002).
18. B.D. Cullity, *Elements of X-ray diffraction* (Massachusetts, USA: Addison-Wesley Inc.: 1956).
19. D.K. Aswal, K.P. Muthe, S. Tawde, S. Chodhury, N. Bagkar, A. Singh, *J. Cryst. Growth* **236**, 661 (2002).
20. B. Sasi, K.G. Gopchandran, *Nanotechnology* **18**, 115613 (2007).
21. M.A. Miller, F.E. Stageberg, Y.M. Chow, K. Rook, L.A. Heuer, *J. Appl. Phys.* **75**, 5779 (1994).
22. A. Sharma, S. Tripathi, N. Lakshmi, P. Sachdev, T. Shripathi, *Solid State Commun.* **149**, 1033 (2009).
23. R. Brajpuria, S. Tripathi, S.M. Chaudhari, *Solid State Commun.* **134**, 479 (2005).
24. A. Hakim, J. Hossain, Khan, *Renew. Energ.* **34**, 2625 (2009).
25. S.A. Makhlouf, *Thin Solid Films* **516**, 3112 (2008).
26. S.A. Makhlouf, M.A. Kaseem, A. Rahim, *J. Mater. Sci.* **44**, 3438 (2009).
27. D. Adler, J. Feinleib, *Phys. Rev. B* **2**, 3112 (1970).
28. F.J. Morin, *Phys. Rev.* **93**, 1199 (1954).
29. P. Lunkenheimer, A.L. Ottermann, K. Bange, *Phys. Rev. B* **44**, 5927 (1991).
30. D.P. Snowden, H. Saltzburg, *Phys. Rev. Lett.* **14**, 497 (1965).
31. N.F. Mott, *J. Non-Cryst. Solids* **1**, 1 (1968).
32. N.F. Mott, *Philo. Mag.* **19**, 835 (1969).
33. G.N. Greaves, *J. Non-Cryst. Solids* **11**, 427 (1973).
34. S.R. Elliot, *Physics of amorphous materials* (Longman London and New York: 1984).
35. M.M. El-Desoky, *J. Mater. Sci.-Mater. Electron.* **14**, 215 (2003).